Check for updates

JGR Atmospheres

RESEARCH ARTICLE
10.1029/2025JD045016

Evaluation of CAM Single-Column Models in Simulating Convectively Coupled Rossby Gravity Waves During TRMM-KWAJEX

Xiaocong Wang[1], Yanjie Liu[2,3], Minghua Zhang[4], Yimin Liu[2], Shuaiqi Tang[5], Zhun Guo[2], Kai Wang[6], and Xiao Zheng[6]

[1]Institute of Atmospheric Physics (IAP), Chinese Academy of Sciences (CAS), Beijing, China, [2]State Key Laboratory of Earth System Numerical Modeling and Application, Institute of Atmospheric Physics, Chinese Academy of Sciences, Beijing, China, [3]College of Earth and Planetary Sciences, University of Chinese Academy of Sciences, Beijing, China, [4]School of Marine and Atmospheric Sciences, Stony Brook University, Stony Brook, New York, USA, [5]School of Atmospheric Sciences, Nanjing University, Nanjing, China, [6]College of Atmospheric Science, Nanjing University of Information Science and Technology, Nanjing, China

Abstract Leveraging observational data from the TRMM-KWAJEX field campaign, which captures the evolution of mixed Rossby-gravity (MRG) waves, this study evaluates how parameterization schemes influence convectively coupled MRG waves in the Community Atmospheric Model single-column framework (SCAM). Four configurations are examined: the traditional approach that uses separate deep (ZM) and shallow (UW) convection schemes (CAM_ZMUW), unified shallow-deep convection (CAM_UNICON), unified cloud-turbulence (CAM_CLUBB), and super-parameterization (CAM_SP). While precipitation is relatively insensitive to parameterization choice, diabatic heating fields differ markedly, which shape temperature, moisture and MRG wave characteristics. All simulations capture the general eastward tilt of MRG waves, but with varying fidelity. CAM_ZMUW and CAM_UNICON produce overly strong convection, while CAM_CLUBB underestimates low-level early-phase moistening. Only CAM_CLUBB and CAM_SP reproduce the successive vertical subgrid-scale transport of moist static energy convergence, though the transport is weaker in CAM_CLUBB, whereas mass-flux-based schemes lack coherent vertical organization. Experiments combining Cloud Layers Unified by Binormals (CLUBB) with ZM deep convection behave similarly to CAM_ZMUW, indicating strong sensitivity to deep-convection scheme. Applying stricter convective triggering in ZM convection alleviates the lower-tropospheric dry bias but does not lead to an improved simulation of the convectively coupled MRG wave. The stochastic Subgrid Importance Latin Hypercube Sampler, a Monte Carlo technique designed to integrate over subgrid variability and improve estimates of its effects on microphysical process rates, has a relatively minor impact on MRG modeling in CLUBB. These results underscore the need to improve the representation of shallow-to-deep convective transitions in mass-flux schemes and to enhance the vertical subgrid-scale transport within the CLUBB framework.

Plain Language Summary Convectively coupled equatorial waves (CCEWs) are essential in modulating tropical weather and climate variability, yet many current weather and climate models struggle to accurately simulate these waves. A major challenge lies in the representation of diabatic heating, which is fundamental to the excitation and maintenance of these waves. In this study, we use observational data from the TRMM-KWAJEX (Tropical Rainfall Measuring Mission–Kwajalein Experiment) field campaign, which captures the evolution of mixed Rossby–gravity (MRG) waves, to evaluate how diabatic heating fields associated with MRG waves are represented under different parameterization schemes. We examine a number of model configurations, ranging from traditional separate physical parameterizations to unified shallow-deep convection and cloud-turbulence schemes, and finally to a super-parameterization approach that explicitly resolves small-scale cloud systems. Our results show that the unified framework improves upon the traditional scheme in capturing the gradual rise of diabatic heating but still falls short of the performance achieved by super-parameterization. These findings provide valuable insights for advancing the representation of tropical wave systems in weather and climate models.

Key Points:

- While precipitation shows limited sensitivity to parameterization choice, the diabatic heating fields exhibit substantial differences
- Parameterization configurations employing the mass-flux schemes lack coherent vertical organization in subgrid-scale moist static energy transport
- Despite exhibiting distinct biases, CLUBB improves upon traditional schemes in capturing the gradual rise of diabatic heating

Supporting Information:

Supporting Information may be found in the online version of this article.

Correspondence to:

X. Wang,
wangxc@lasg.iap.ac.cn

Citation:

Wang, X., Liu, Y., Zhang, M., Liu, Y., Tang, S., Guo, Z., et al. (2026). Evaluation of CAM single-column models in simulating convectively coupled Rossby gravity waves during TRMM-KWAJEX. *Journal of Geophysical Research: Atmospheres*, *131*, e2025JD045016. https://doi.org/10.1029/2025JD045016

Received 1 AUG 2025
Accepted 1 FEB 2026

© 2026. The Author(s).
This is an open access article under the terms of the Creative Commons Attribution License, which permits use, distribution and reproduction in any medium, provided the original work is properly cited.

21698996, 2026, 4, Downloaded from https://agupubs.onlinelibrary.wiley.com/doi/10.1029/2025JD045016 by Xiaocong Wang, Wiley Online Library on [12/02/2026]. See the Terms and Conditions (https://onlinelibrary.wiley.com/terms-and-conditions) on Wiley Online Library for rules of use; OA articles are governed by the applicable Creative Commons License

1. Introduction

Convectively coupled equatorial waves (CCEWs) have long been recognized as fundamental components of weather and climate in the tropics, playing a critical role in organizing deep convection and serving as key drivers of subseasonal predictability through their modulation on large-scale circulation patterns (Cheng et al., 2023; Dias & Kiladis, 2019; Kiladis et al., 2009). However, accurately simulating these waves in general circulation models (GCMs) remains a persistent challenge. GCMs typically suffer from poor simulations of CCEWs in terms of wave amplitude, phase speed, and the front-to-rear tilting wave structure (Huang et al., 2013; Lin et al., 2006; Wang & Li, 2017), despite progress made over the past few decades (Dias et al., 2023; Schreck et al., 2020). A major challenge lies in accurately representing diabatic heating, which is crucial for the excitation and maintenance of CCEWs. Theoretical studies highlighted the pivotal role of interactions among planet boundary layer (PBL) turbulence, shallow and deep convection, and stratiform condensation processes in shaping diabatic heating structures (Kuang, 2008; Majda & Shefter, 2001; Mapes, 2000). However, GCMs often struggle to adequately represent critical interactions among these processes, particularly the transition from shallow to deep convection, resulting in misrepresentation of timing of convection and, consequently, the associated diabatic heating fields (Krishnamurti et al., 2007; Yuan et al., 2013). This issue is also evident in reanalysis products (Wang & Zhang, 2024), which are influenced by the GCMs used in their generation. A contributing factor is that individual parameterization schemes are often developed in isolation, leading to inconsistencies and disconnections among model components (Donahue & Caldwell, 2018; Wang & Zhang, 2013). To remedy this problem, there has been a growing emphasis on developing unified parameterization frameworks that treat physical processes as an integrated system (Golaz et al., 2002; Neggers et al., 2009; Park, 2014a). To what extent can unified parameterizations improve the simulation of CCEWs? Exploring the answer to this question inspires this study.

Previous assessments of CCEWs primarily relied on global or regional models (Hung et al., 2013; Wang & Li, 2017), in which complex interplay between model dynamics and physics often obscures the attribution of simulation errors. In contrast, single-column models (SCMs), which employ externally prescribed large-scale forcings (Randall et al., 1996), offer an alternative controlled framework for isolating and systematically assessing the performance of parameterization schemes in simulating CCEWs. This enables a close scrutiny of the responses of parameterized subgrid physical processes to large-scale forcings in an isolated manner. Using meteorological fields derived from constrained variational analysis (Zhang et al., 2001; Zhang & Lin, 1997), Wang and Zhang (2015) identified distinct mixed Rossby-gravity (MRG) waves during the Tropical Rainfall Measuring Mission—Kwajalein Experiment field campaign (TRMM-KWAJEX; Sobel et al., 2004; Schumacher et al., 2007, 2008). The unique data set enables an unprecedented evaluation of parameterization schemes for simulating MRG waves within SCMs.

Using the TRMM-KWAJEX case that captures the evolution of MRG waves, this study investigates the behavior and interactions of individual parameterizations across different phases of the MRG wave. Specifically, we evaluate the simulated diabatic heating fields under different parameterization schemes within the SCM framework and compare them against observations. The paper is structured as follows: Section 2 describes the case setup, model configurations, and experimental design. Section 3 evaluates the general performance of different parameterization configurations in simulating precipitation, temperature and moisture, and diabatic heating. Section 4 presents a comparison of composite anomalies in temperature, moisture, precipitation, apparent heat source, moisture sink, and the subgrid-scale vertical transport of moist static energy (MSE) convergence of MRG waves between simulations and observations. Results of the sensitivity experiments are provided in Section 5, followed by a summary of the main conclusions in Section 6.

2. Case, Model, and Experiments

2.1. Case Description

The KWAJEX field campaign was conducted near the Kwajalein Atoll in the Republic of the Marshall Islands (7°–10°N, 166°–169°E) from 24 July to 15 September 1999. Numerous studies have utilized its comprehensive observing network—including aircraft, upper-air soundings, ships, and an array of surface-based remote and in situ sensors—to analyze the region's meteorology and precipitation (e.g., Schumacher et al., 2007, 2008; Sobel et al., 2004). To produce the large-scale forcing suitable for driving SCM and cloud-resolving model (CRM), upper-air observations from the campaign were processed through variational analysis constrained by the conservation of column-integrated mass, moisture, and energy (Tang & Zhang, 2015; Zhang et al., 2001; Zhang &

Table 1
Parameterization Configurations

Parameterization	CAM_ZMUW	CAM_UNICON	CAM_CLUBB	CAM_SP
PBL turbulence	Bretherton and Park (2009)	Bretherton and Park (2009)		
Shallow convection	Bretherton and Park (2008)	Park (2014a)	Golaz et al. (2002)	Khairoutdinov and Randall (2001)
Deep convection	Zhang and McFarlane (1995)			
Cloud macrophysics	Park et al. (2014)	Park et al. (2014)		
Cloud microphysics	Morrison and Gettelman (2008)			
Radiation	Clough et al. (2005)			

Lin, 1997). Utilizing this data set, Wang and Zhang (2015) constructed a composite of convectively coupled MRG waves and investigated the interactions between MRG dynamics and diabatic heating across all wave phases. This benchmark case has been widely employed in cloud-resolving modeling studies on convection and cloud processes (e.g., Blossey et al., 2007; Wang, 2022; Zhao et al., 2024). In this study, we use this unique data set to drive SCMs to explore how individual parameterization schemes behave and interact with one another across different MRG phases.

2.2. Model and Experimental Design

We conduct KWAJEX simulations using the single-column version of the Community Atmospheric Model (SCAM). The latest SCAM framework (Gettelman et al., 2019) features a number of parameterization schemes for PBL turbulence and cumulus convection, ranging from traditional separate schemes to unified shallow-deep convection and cloud–turbulence schemes, and to super-parameterizations. There is a substantial body of work dedicated to the systematic evaluation of parameterization suits (e.g., Bogenschutz et al., 2018; Lin et al., 2019). In this study, four distinct configurations are evaluated: CAM_ZMUW, CAM_UNICON, CAM_CLUBB, and CAM_SP. In the CAM_ZMUW setup, deep convection is parameterized using the Zhang and McFarlane (1995) scheme, while PBL turbulence and shallow convection are treated with Park and Bretherton (2009) scheme. CAM_UNICON employs a unified framework for both shallow and deep convection (Park, 2014a), and parameterizes PBL turbulence following Bretherton and Park (2009). The CAM_CLUBB configuration employs the Cloud Layers Unified by Binormals (CLUBB) scheme (Golaz et al., 2002; Guo et al., 2021), a unified parameterization that integrates clouds and turbulence through a single set of prognostic equations (Larson et al., 2002). In this setup, CLUBB is further extended to replace the *Zhang-McFarlane* deep convection scheme, following an approach similar to that of Guo et al. (2015). The performance of two additional CLUBB configurations is presented in Section 4.3. The super-parameterized configuration (CAM_SP) employs the Multiscale Modeling Framework, embedding a CRM with kilometer-scale resolution in each grid column of the host model (Khairoutdinov & Randall, 2001; Lin et al., 2018; Wang et al., 2011). This approach explicitly resolves small cloud systems, thereby eliminating the need for traditional subgrid-scale parameterizations. Other parameterizations are set the same across all configurations. Cloud microphysics is represented by the Morrison and Gettelman (2008) scheme, which predicts both mixing ratios and number concentrations for suspended and precipitating hydrometeors. Radiative transfer is handled using the Rapid Radiative Transfer Model for GCMs (RRTMG; Clough et al., 2005). Table 1 summarizes the key differences in parameterization components across different configurations. For benchmarking and process-level evaluation, we also perform CRM simulations using the System for Atmospheric Modeling (SAM v6.9.4, Khairoutdinov & Randall, 2003), which is identical to the embedded CRM in CAM_SP, but with finer horizontal resolution −256 × 256 subcolumns with 1 km grid spacing, compared to 32 × 32 subcolumns with 8 km spacing in CAM_SP. In SAM, subgrid-scale turbulence is represented using a 1.5-order closure with prognostic turbulent kinetic energy. The model is configured with 64 vertical levels, featuring a grid spacing that increases gradually from 75 m at the surface to 400 m through the troposphere, and further to 1 km in the Newtonian damping layer. The horizontal domain spans 256 × 256 grid points with 1 km resolution, and the time step is set to 10 s. The large-scale forcing used to drive SACM and SAM —including horizontal advective tendencies and vertical velocity—is derived from the objectively constrained variational analysis of Zhang and Lin (1997). To reduce error accumulation, all simulations are restarted at 06 UTC every day from July 24 to September 15 for a 36-hr integration using 3-hr momentum nudging but excluding relaxation for other variables, and the last 24-hr simulations are used for analysis.

21698996, 2026, 4, Downloaded from https://agupubs.onlinelibrary.wiley.com/doi/10.1029/2025JD045016 by Xiaocong Wang , Wiley Online Library on [12/02/2026]. See the Terms and Conditions (https://onlinelibrary.wiley.com/terms-and-conditions) on Wiley Online Library for rules of use; OA articles are governed by the applicable Creative Commons License

21698996, 2026, 4, Downloaded from https://agupubs.onlinelibrary.wiley.com/doi/10.1029/2025JD045016 by Xiaocong Wang, Wiley Online Library on [12/02/2026]. See the Terms and Conditions (https://onlinelibrary.wiley.com/terms-and-conditions) on Wiley Online Library for rules of use; OA articles are governed by the applicable Creative Commons License

3. Evaluation of Precipitation, Diabatic Heating, and Thermodynamic Fields

Before examining the characteristics of convectively coupled MRG waves, we first perform a comprehensive evaluation of SCAM performance in simulating precipitation, diabatic heating, temperature, and moisture fields. This assessment aims to clarify the influence of different parameterization schemes on the overall model behavior.

3.1. Precipitation and Diabatic Heating

Figure 1 presents the observed and simulated surface precipitation from the different SCM configurations, plotted in consecutive panels for the entire period for clarity. Overall, all simulations successfully capture the temporal evolution of observed precipitation, with correlation coefficients exceeding 0.83, although they consistently underestimate the intensity during peak convective periods except CAM_UNICON. This general agreement arises because the imposed observational forcing constrains the models to satisfy the energy and moisture budget equation, thereby producing precipitation similar to observations (Tang et al., 2017; Wang, 2015; Wang et al., 2015). Models exhibit greater divergence in simulating moderate precipitation, revealing that under relatively weak large-scale forcing, the solutions become increasingly sensitive to the specific formulation of convective representation. Comparatively, CAM_UNICON produces the highest precipitation (8.31 mm/day), whereas CAM_CLUBB yields the lowest (4.30 mm/day). CAM_ZMUW and CAM_SP fall between these extremes (6.74 and 6.26 mm/day, respectively), with CAM_SP being closest to the observed value of 6.14 mm/day. The strong precipitation simulated by CAM_UNICON is consistent with Park (2014b) and may be attributed to positive perturbations in updraft vertical velocity, temperature, and moisture in response to mesoscale organized flow.

While the simulated precipitation shows weak sensitivity to parameterization configurations, the vertical structure of diabatic heating exhibits pronounced differences. Figure 2 compares the period-averaged apparent heating Q_1, moisture sink Q_2, and their component contributions from individual parameterizations in each SCAM. The observed Q_1 and Q_2 are derived as residuals of the thermodynamic equation and water vapor mass continuity equation from the variational objective analysis (Zhang & Lin, 1997), whereas the simulated Q_1 and Q_2 are computed as the sum of tendencies from individual parameterizations. CAM_ZMUW exhibits a positive bias of approximately 1 K/day in Q_1 within the mid-troposphere and a negative bias of approximately 2 K/day in Q_2 in the lower troposphere compared to observations (blue line in Figure 2a). CAM_UNICON produces even stronger Q_1 and Q_2 than CAM_ZMUW. In contrast, CAM_CLUBB produces weaker Q_1—especially in the mid-to upper troposphere—and substantially underestimates Q_2 throughout the column, consistent with its lower precipitation (Figure 1). The Q_1 and Q_2 biases in CAM_CLUBB (<0.5 K/day) are notably smaller than those in CAM_ZMUW (>1 K/day). Among all four simulations, CAM_SP bears the closest resemblance to observations, with deviations in Q_1 and Q_2 mostly within the range of 0.2 K/day. The overestimation of Q_1 in CAM_ZMUW and CAM_UNICON largely results from excessive deep convective heating (pink solid line in Figures 2b and 2c), which peaks around 4 K/day. Concurrently, excessive convection induces substantial drying of the lower troposphere, which is then partially offset by moisture supplies from PBL turbulence and shallow convection (green dash line in Figures 2b and 2c). The stratiform process in CAM_ZMUW is characterized by low-level cooling and moistening due to evaporative processes, along with a secondary, smaller warming-drying peak in upper levels. In contrast, CAM_UNICON exhibits column-wide moistening driven by evaporation, except in the upper troposphere where condensation dominates. With regard to CAM_CLUBB, heating from the CLUBB scheme (green solid line in Figure 2d) peaks near 700 hPa, and decreases more rapidly with height, terminating around 450 hPa. This shallower vertical extent suggests reduced vertical penetration relative to the mass-flux scheme (pink solid line in Figures 2b and 2c). The insufficient heating in the upper troposphere is partially compensated by an enhancement in stratiform heating, which peaks near 350 hPa at about 1.8 K/day—much larger than those seen in CAM_ZMUW and CAM_UNICON. This occurs because stratiform microphysics takes up the release of latent heat that is left over by CLUBB, whereas CAM_ZMUW and CAM_UNICON rely primarily on their convection schemes to release latent heat. Radiative cooling dominates the upper-tropospheric Q_1 budget in all experiments except CAM_UNICON, where strong longwave cooling largely offsets diabatic heating from moist processes. In contrast, CAM_UNICON exhibits distinct radiative heating near 200–300 hPa. This signal stems from enhanced longwave heating below cloud top, which is associated with the scheme's excessive production of high-cloud fraction, as will be shown in Figure 4.

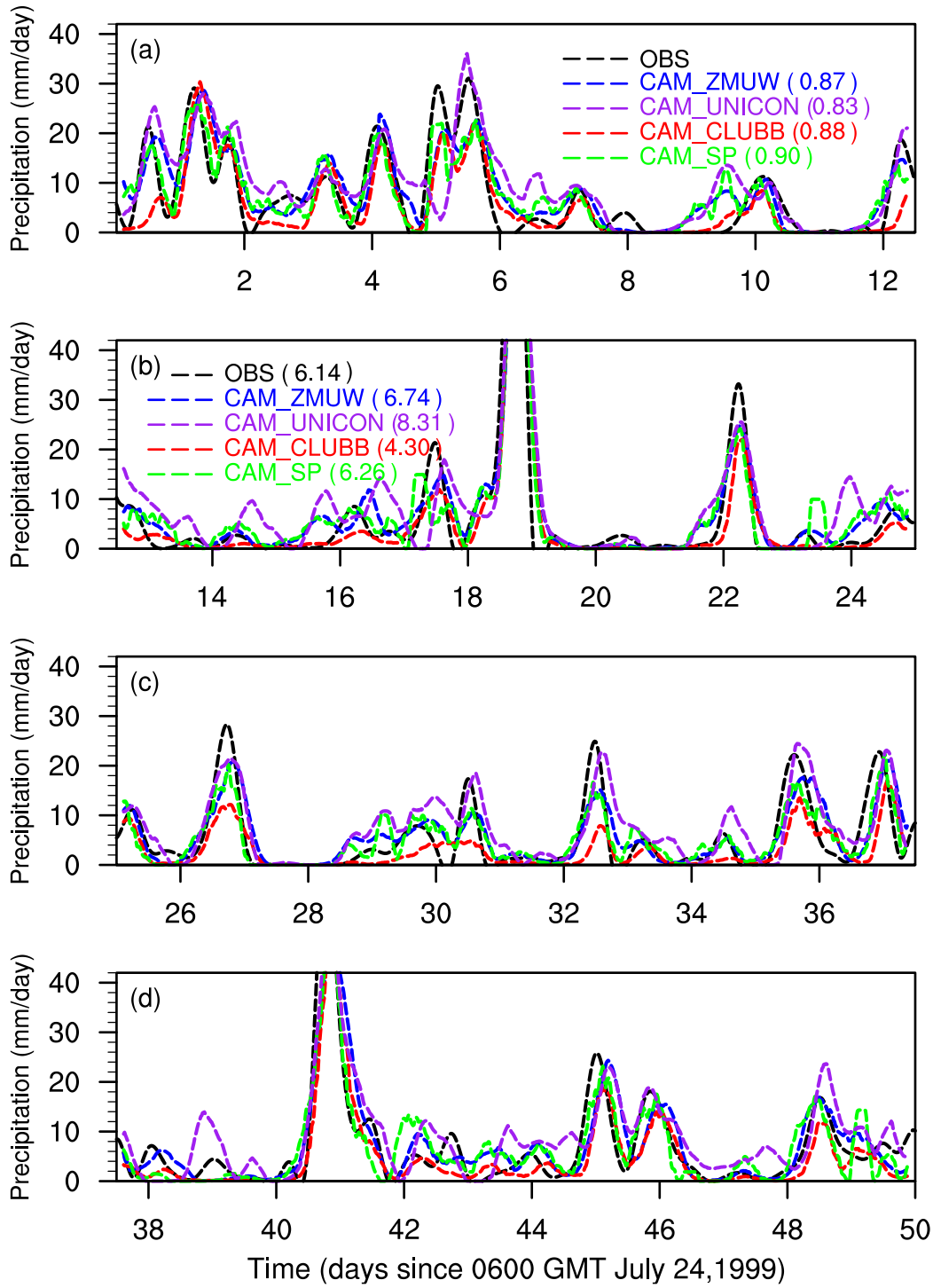


Figure 1. Time series of observed and simulated surface precipitation rates during the KWAJEX field campaign, as produced by CAM single-column models configured with different physical parameterization schemes. The blue line represents simulations using traditional separate physical schemes (CAM_ZMUW), the purple line corresponds to simulations with the UNICON scheme (CAM_UNICON), the red line denotes simulations with the unified CLUBB scheme (CAM_CLUBB), and the green line shows results from the super-parameterized configuration (CAM_SP). The numbers in (a) and (b) represent the temporal correlation coefficients and period-averaged precipitation, respectively. Units are in mm/day.

21698996, 2026, 4, Downloaded from https://agupubs.onlinelibrary.wiley.com/doi/10.1029/2025JD045016 by Xiaocong Wang , Wiley Online Library on [12/02/2026]. See the Terms and Conditions (https://onlinelibrary.wiley.com/terms-and-conditions) on Wiley Online Library for rules of use; OA articles are governed by the applicable Creative Commons License

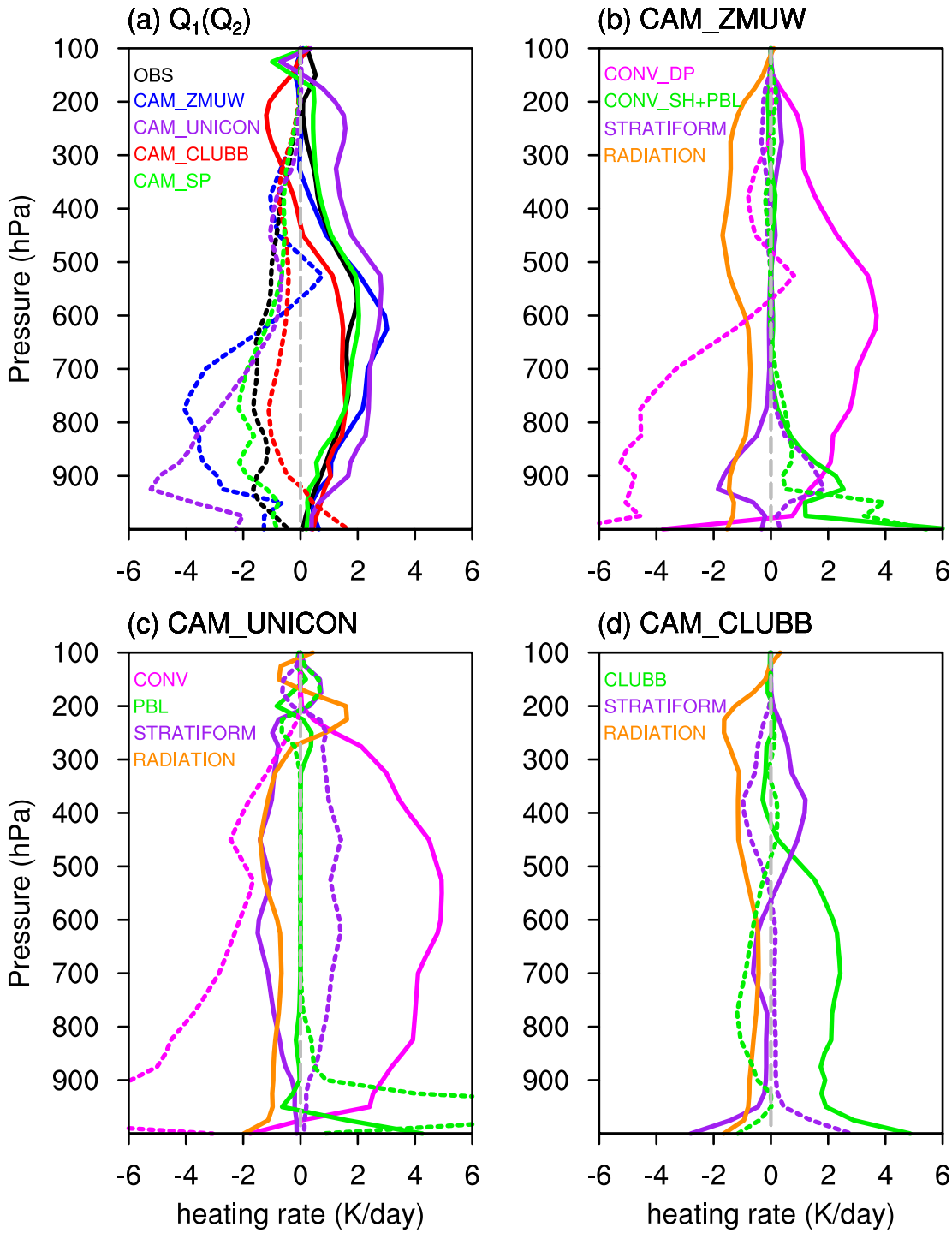


Figure 2. Apparent heat source (solid lines) and moisture sink (dashed lines) from observations and simulations (a), along with their respective components for CAM_ZMUW (b), CAM_UNICON (c) and CAM_CLUBB (d). Units: K/day.

3.2. Temperature, Moisture, and Clouds

Figure 3 shows the differences in temperature, specific humidity, and relative humidity between simulations and observations. The analysis is restricted to levels below 200 hPa due to substantial uncertainties in the imposed forcing at upper layers (Wang & Zhang, 2013). CAM_ZMUW exhibits a band of warm bias of up to 3 K in the mid-troposphere, flanked by cold biases of up to 2 K above and below, whereas CAM_UNICON shows a warm

21698996, 2026, 4, Downloaded from https://agupubs.onlinelibrary.wiley.com/doi/10.1029/2025JD045016 by Xiaocong Wang , Wiley Online Library on [12/02/2026]. See the Terms and Conditions (https://onlinelibrary.wiley.com/terms-and-conditions) on Wiley Online Library for rules of use; OA articles are governed by the applicable Creative Commons License

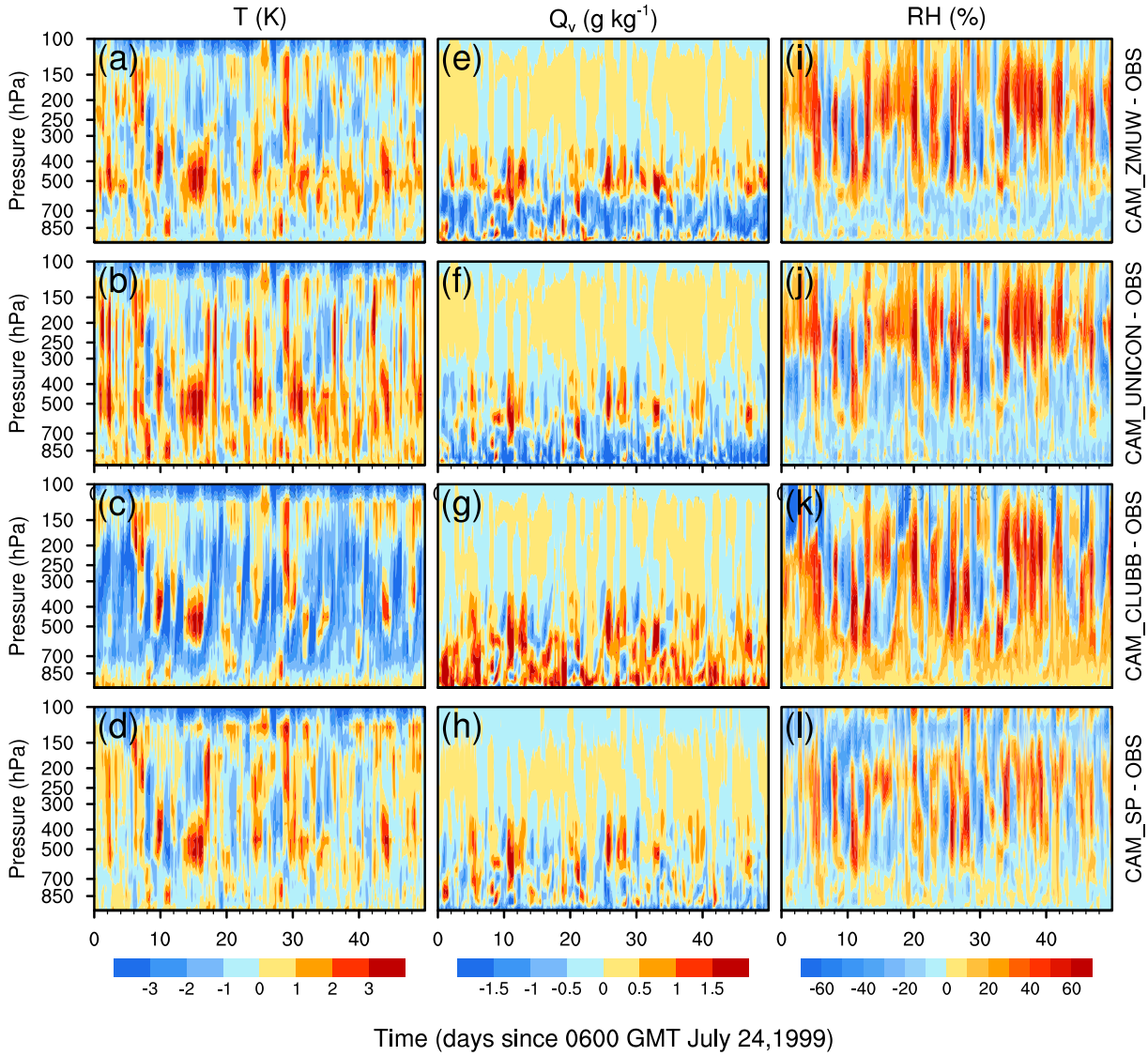


Figure 3. Temperature, moisture, and relative humidity biases between observation and simulations by (a, e, i) CAM_ZMUW (b, f, j) CAM_UNICON (c, g, k) CAM_CLUBB, and (d, h, l) CAM_SP. Units: K for temperature, g/kg for moisture, and % for relative humidity.

bias confined to the lower and mid-troposphere. Meanwhile, both models exhibit a pronounced moist bias of up to 1.5 g/kg above 600 hPa and a dry bias of similar magnitude in the lower troposphere. Notably, the dry bias is moderately reduced in CAM_UNICON compared to CAM_ZMUW. These bias patterns align with known limitations of the CAM model (Ma et al., 2021; Wang & Zhang, 2013; Xie et al., 2012; Xie & Zhang, 2000), which are primarily attributed to overly active deep convection. In the lower troposphere, cold-dry and warm-moist biases exhibit strong covariation, leading to relative humidity biases mostly within 10%. In contrast, CAM_CLUBB exhibits a widespread cold bias of up to 2 K throughout the troposphere, accompanied by significant moist biases reaching 1.5 g/kg below 500 hPa. The issue of excessive tropical water vapor when using CLUBB to replace deep convection schemes has also been noted by Guo et al. (2015). These biases stem largely from CLUBB's reduced efficiency in vertically transporting moisture, which represents non-local transport by transporting parcels a little bit over each of many short time steps—an approach conceptually distinct from the schemes used in traditional parameterizations (Larson, 2017). At lower levels, the combination of cooler temperature and higher moisture leads to relative humidity biases exceeding 20%. CAM_SP, on the other hand, aligns most closely with observations, with temperature and moisture deviations mostly within ±1 K and ±0.5 g/kg, respectively.

21698996, 2026, 4, Downloaded from https://agupubs.onlinelibrary.wiley.com/doi/10.1029/2025JD045016 by Xiaocong Wang , Wiley Online Library on [12/02/2026]. See the Terms and Conditions (https://onlinelibrary.wiley.com/terms-and-conditions) on Wiley Online Library for rules of use; OA articles are governed by the applicable Creative Commons License

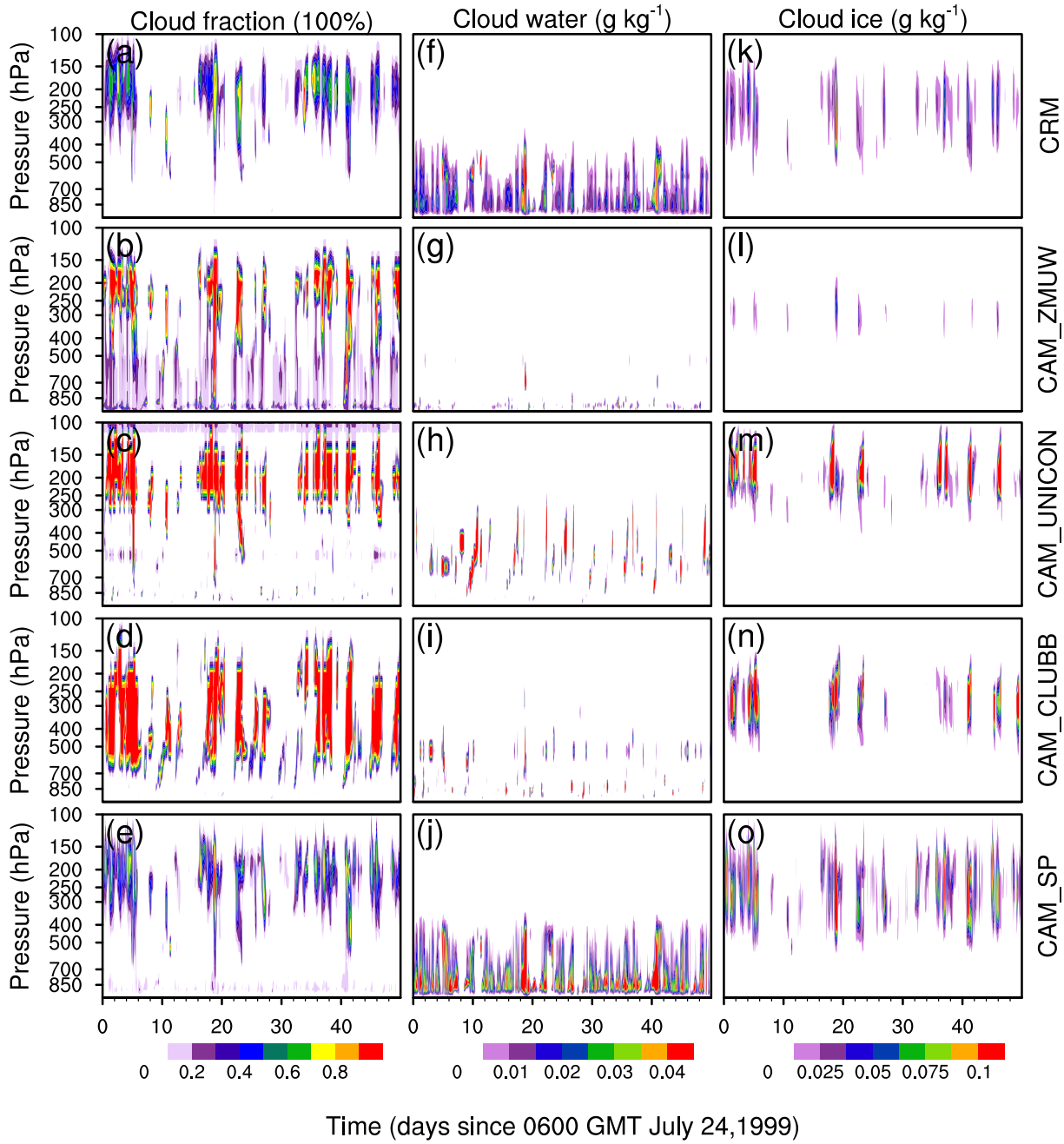


Figure 4. Simulated Cloud fraction, cloud water, and cloud ice from the CRM ensemble mean (a, f, k), and from the SCM simulations using CAM ZMUW (b, g, l), CAM UNICON (c, h, m), CAM CLUBB (d, i, n), and CAM SP (e, j, o). Units: 100% for cloud fraction and g/kg for cloud water and ice.

Figure 4 compares cloud fraction, cloud liquid water, and ice content across the four SCAM configurations, using the SAM simulation as a benchmark. To minimize uncertainty associated with the CRM's microphysical parameterization, the CRM benchmark is taken as an ensemble mean of three distinct microphysics schemes: the single-moment scheme SAM1MOM (Khairoutdinov & Randall, 2003), the bulk parameterization LIN (Lin et al., 1983), and the double-moment scheme M2005 (Morrison et al., 2005). The individual results from these schemes are provided in Figure S1 in Supporting Information S1. Still, it must be acknowledged that the CRM simulation serves as a useful but imperfect reference in the absence of comprehensive cloud condensate observations. As shown in Figure 4, the CRM simulation exhibits prominent cloud ice concentrations in the upper troposphere. Cloud liquid water comprises approximately half the mass of the ice content and is mostly confined

21698996, 2026, 4, Downloaded from https://agupubs.onlinelibrary.wiley.com/doi/10.1029/2025JD045016 by Xiaocong Wang , Wiley Online Library on [12/02/2026]. See the Terms and Conditions (https://onlinelibrary.wiley.com/terms-and-conditions) on Wiley Online Library for rules of use; OA articles are governed by the applicable Creative Commons License

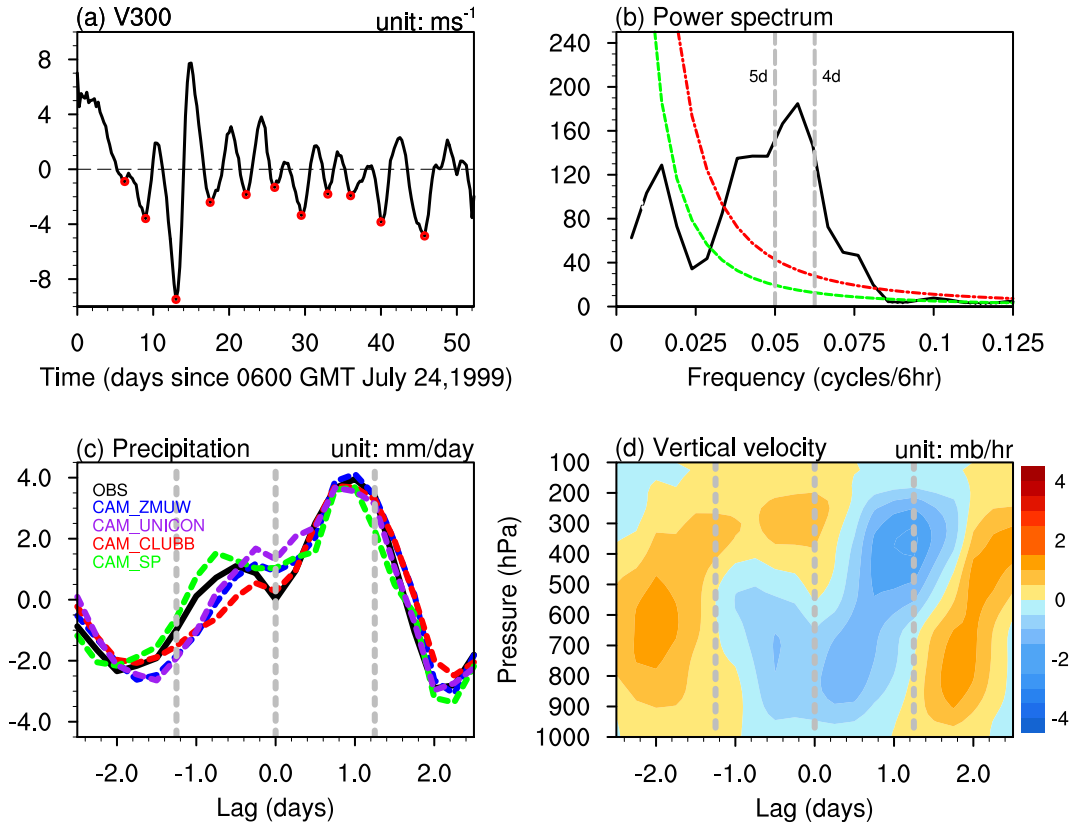


Figure 5. (a) Observed meridional wind at 300 hPa after the removal of time average and diurnal cycle (unit: m/s). (b) Power spectrum of the observed 300 hPa meridional wind (unit: m^2/s^2). (c) Composite anomalies of observed and simulated precipitation (units: mm/day). (d) Composite anomaly of vertical velocity from observations (units: hPa/h). The red and green curves in (b) denote "Red Noise" spectrum and 95% confidence for Markov, respectively.

below 500 hPa (note the differing color scales used for liquid and ice concentrations). The vertical structure of cloud fraction mirrors that of cloud ice, with relatively less presence in lower layers. Compared to CRM, all simulations except CAM_SP substantially overestimate cloud fraction, especially for high-level clouds. CAM_ZMUW severely underestimates both cloud liquid and ice water content. This inverse relationship—overestimated cloud coverage but underestimated condensate—suggests the presence of optically thin clouds in CAM_ZMUW, consistent with Park et al. (2014). Among all simulations, CAM_SP most closely resembles the CRM results, despite using only one-eighth the number of subcolumns used in the latter. Note this approach may inherently favor the CAM_SP simulation, since CAM_SP embeds the same CRM used as the benchmark.

4. Evaluation of Composite Structure of MRG Waves

The preceding section critically evaluated the performance of different parameterization schemes in simulating moist physical processes. This section explores how these schemes influence MRG waves, with particular emphasis on their coupling with diabatic heating. We begin by briefly reviewing the MRG waves identified from observations in Wang and Zhang (2015). Figure 5a shows the time series of 300 hPa meridional winds, with both the diurnal cycle and time-mean components removed. Alternating southerly and northerly winds appear at intervals of 4–5 days, with a dominant power spectral peak at 4.5 days (Figure 5b). This period aligns with previously reported MRG wave characteristics in the equatorial Pacific (e.g., Straub & Kiladis, 2003; Swann et al., 2006). Figure 5c presents 5-day composites of observed and simulated precipitation anomalies, where day 0 corresponds to the time of minima meridional wind at 300 hPa, marked in red in Figure 5a. The MRG cycle is divided into four phases, indicated by dashed gray lines. Precipitation begins to increase at the end of Phase 1, intensifies through Phase 2 and 3, and then collapses abruptly in Phase 4. The evolution of precipitation closely coincides with that of large-scale vertical velocity, which shows anomalous ascent in Phase 2 and 3 and descent in

21698996, 2026, 4, Downloaded from https://agupubs.onlinelibrary.wiley.com/doi/10.1029/2025JD045016 by Xiaocong Wang , Wiley Online Library on [12/02/2026]. See the Terms and Conditions (https://onlinelibrary.wiley.com/terms-and-conditions) on Wiley Online Library for rules of use; OA articles are governed by the applicable Creative Commons License

21698996, 2026, 4, Downloaded from https://agupubs.onlinelibrary.wiley.com/doi/10.1029/2025JD045016 by Xiaocong Wang , Wiley Online Library on [12/02/2026]. See the Terms and Conditions (https://onlinelibrary.wiley.com/terms-and-conditions) on Wiley Online Library for rules of use; OA articles are governed by the applicable Creative Commons License

Phase 1 and 4 (Figure 5d). This result is not surprising, as simulated precipitation is predominantly controlled by large-scale forcing—particularly vertical velocity—given the relative invariance of the lapse rate and radiative cooling in the tropics (Sobel & Bretherton, 2000). All four simulations reproduce the phase-locked evolution of precipitation reasonably well. It is worth noting all three parameterized experiments show a delayed peak in congestus precipitation, while CAM_SP shows the precipitation peak ahead of the observation. This demonstrates that under relatively weak large-scale forcing, the model solutions become more sensitive to the details of convection representation, resulting in greater diversity in the simulated timing of convective peaks.

4.1. Composite Structure of Temperature, Moisture, and Relative Humidity

Figure 6 compares the 5-day composites of temperature, moisture and relative humidity between observations and SCM simulations. The observed temperature anomalies manifest a vertically eastward-tilting structure, with a sharp phase transition around 500 hPa. Only CAM_CLUBB roughly reproduces the eastward-tilting structure below 500 hPa, while all other simulations exhibit a westward tilt instead. Overall, the simulated temperature composites by SCM are less accurate than those derived from reanalysis shown in Wang and Zhang (2024), likely due to data assimilation in reanalyses across the temporal and spatial scales of MRG waves. Furthermore, the SCM framework inherently lacks two-way interaction. This limitation prevents dynamic adjustments of the circulation to local processes, which may also contribute to the simulated biases. For specific humidity, observations reveal a gradual vertical progression, with moistening beginning near the surface in Phase 1, intensifying between 600 and 700 hPa in Phase 2, and peaking between 400 and 500 hPa in Phase 3. CAM_ZMUW, CAM_UNICON and CAM_SP accurately capture this structure, whereas CAM_CLUBB fails to adequately simulate the surface moistening anomaly during Phase 2. Notably, only CAM_ZMUW captures the peak of positive moisture around 500 hPa—a feature missed by all other configuration suites. The bias of moisture then carries over to that of relative humidity, resulting in structural patterns that closely resemble those seen in specific humidity.

4.2. Composite Structure of Diabatic Heating

To examine the diabatic heating processes associated with MRG waves, Figure 7 presents composite anomalies of the apparent heat source Q_1 and moisture sink Q_2. The observed Q_1 becomes positive in Phase 2, with maximum heating confined below 600 hPa. This shallow convective heating is in line with mid-tropospheric subsidence (Figure 5d), which inhibits the ascent of cumulus parcels. In Phase 3, deep convection produces a pronounced heating center in the upper troposphere, followed by stratiform-like heating with upper-level warming and lower-level cooling. Subsequently, a cold anomaly emerges in Phase 4, indicating the demise of convection. Such an evolution of diabatic heating is also suggested in other tropical systems (e.g., Feng et al., 2020; Straub & Kiladis, 2003). While all SCMs reasonably capture the deep convective heating in Phase 3, they generally struggle to accurately represent the shallow convective heating in Phase 2. All four simulations commonly underestimate the height of the congestus top. Besides, CAM_ZMUW and CAM_SP tend to overestimate the heating anomaly, while CAM_CLUBB tends to underestimate it. Model–observation agreement is even weaker for Q_2 than Q_1, though all SCMs generally reproduce the observed eastward-tilting structure to some extent. Observations reveal two maxima in Q_2: one in the lower troposphere caused by vertical divergence of moisture through PBL turbulence and shallow convection, and the other in the upper troposphere due to cloud condensation. CAM_ZMUW substantially overestimates the lower-level Q_2 (3 K/day vs. the observed 2 K/day)—consistent with its overly vigorous convective transport and the coincident dry bias in Figure 3d. The overestimation of Q_2 is however much alleviated in CAM_UNICON. CAM_CLUBB produces a more organized structure than CAM_ZMUW but struggles to replicate the observed dual-peak pattern, suggesting inadequate subgrid-scale moisture transport and deficient representation of ice-phase processes (e.g., depositional growth and sublimation of ice crystals) critical for stratiform heating, particularly during periods of active convection. Overall, CAM_UNICON and CAM_SP show the closest agreement with observations among all four SCMs.

A comparison of the Q_1 and Q_2 provides further insights into the coupling between diabatic heating and wave dynamics. For the majority of Phases 2 and 3, Q_1 and Q_2 are concurrently positive, indicative of predominant condensational heating in shallow and deep convection. However, during the initial stage of Phase 2, Q_2 is negative while Q_1 is positive, a feature that can only be explained by moisture convergence through vertical turbulent transport by PBL turbulence and/or shallow convection. This interpretation is supported by the

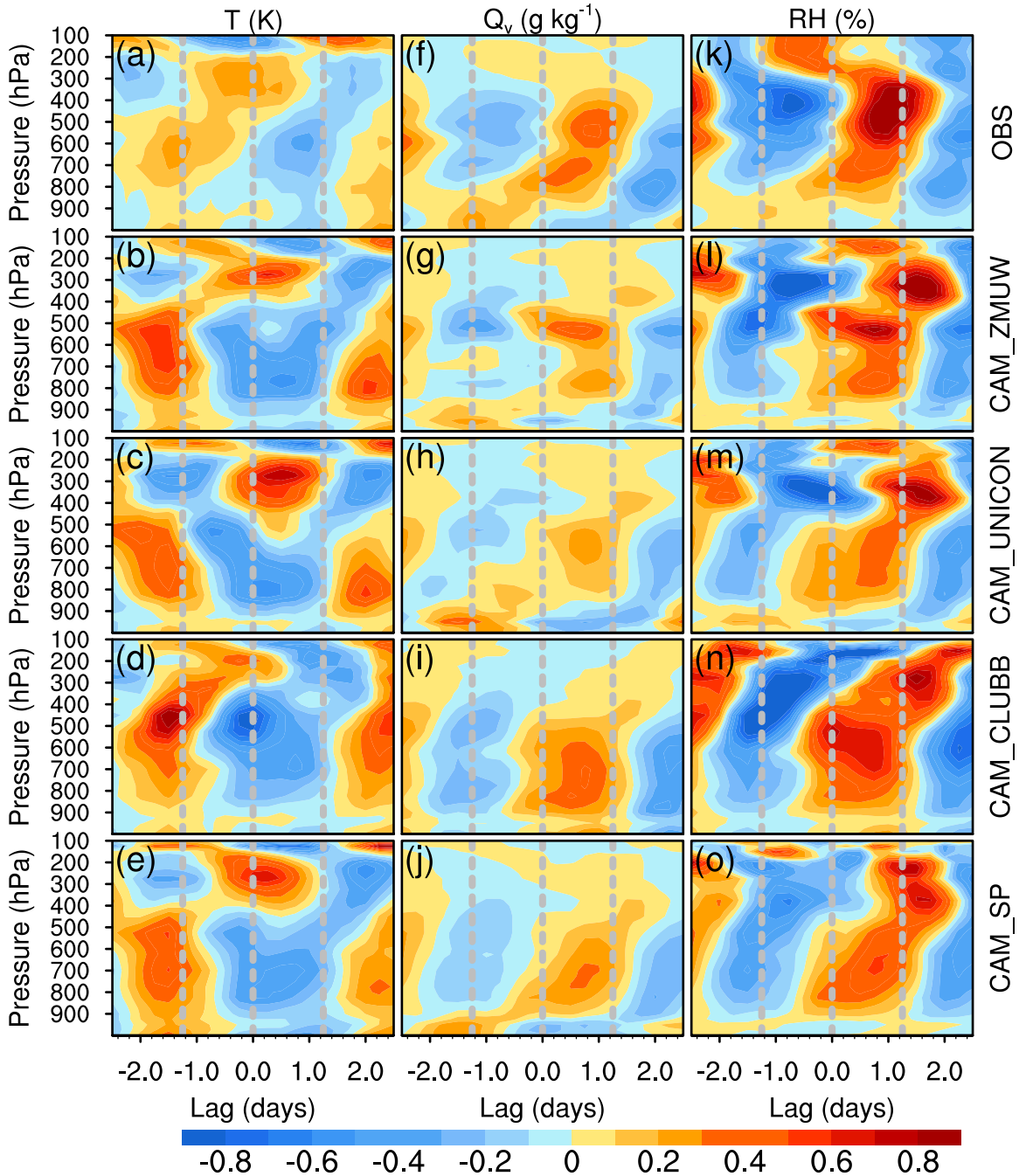


Figure 6. Composite anomalies of observed and simulated temperature (a–e), specific humidity (f–j), and relative humidity (k–o). Units: K for temperature, g/kg for moisture, and % for relative humidity.

$Q_1 - Q_2 - Q_{rad}$ field shown in the rightmost column of Figure 7, which represents the vertical subgrid-scale transport of MSE convergence, expressed as

$$Q_1 - Q_2 - Q_{rad} = -\frac{\partial \overline{\omega' h'}}{\partial p}$$

where Q_{rad} denotes the radiative heating rate, h stands for MSE. In Phase one, $Q_1 - Q_2 - Q_{rad}$ is initially positive and continues to rise due to convective eddy transport from shallow convection. As the cycle progresses,

21698996, 2026, 4, Downloaded from https://agupubs.onlinelibrary.wiley.com/doi/10.1029/2025JD045016 by Xiaocong Wang , Wiley Online Library on [12/02/2026]. See the Terms and Conditions (https://onlinelibrary.wiley.com/terms-and-conditions) on Wiley Online Library for rules of use; OA articles are governed by the applicable Creative Commons License

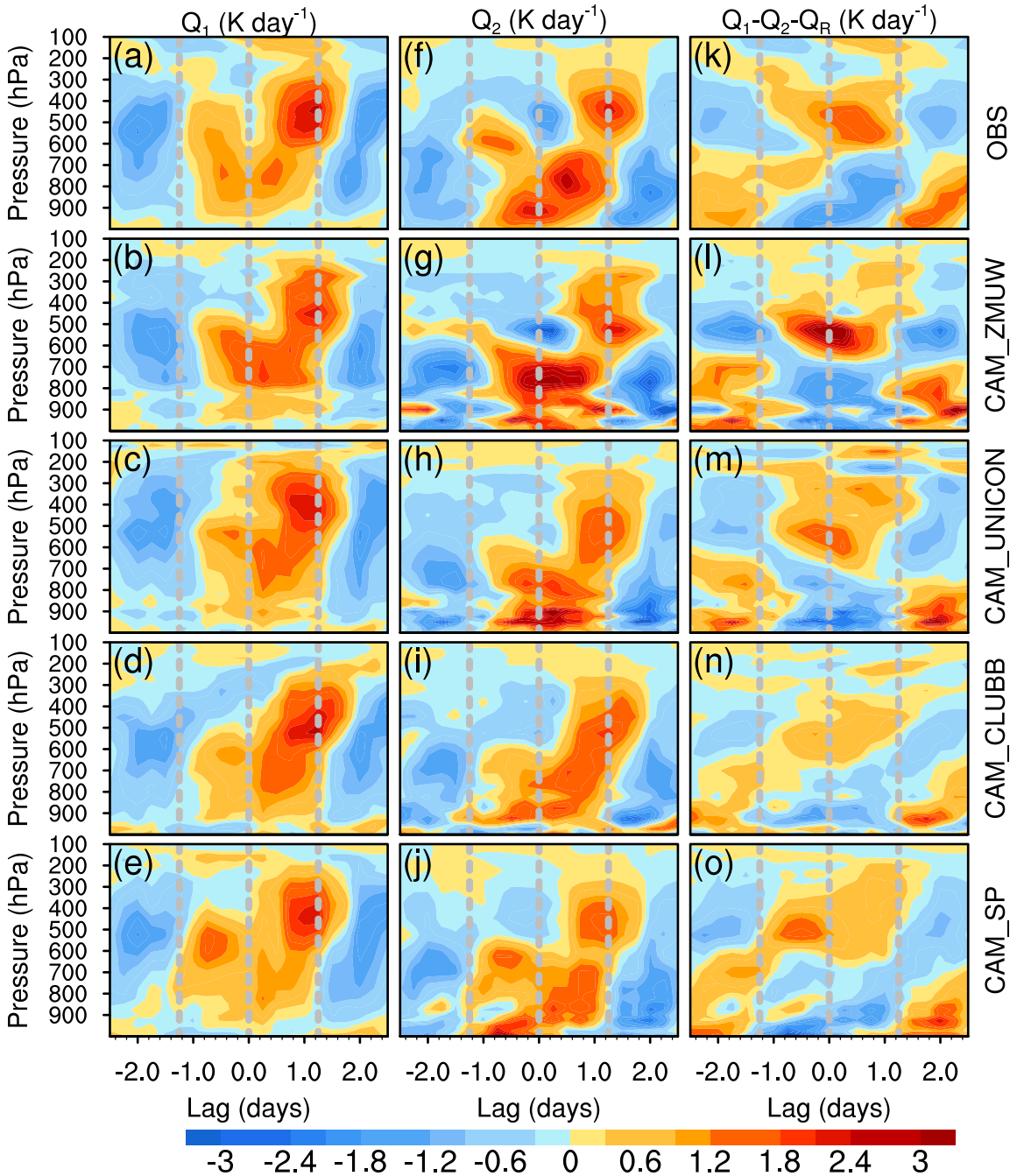


Figure 7. Same as Figure 6 except for the fields of apparent heating Q_1 (a–e), moisture sink Q_2 (f–j), and subgrid-scale vertical transport of moist static energy convergence $Q_1 - Q_2 - Q_{rad}$ (k–o). Units: K/day.

a characteristic dipole structure emerges in its vertical profile—negative anomalies dominate below 600 hPa, while positive anomalies prevail aloft—a typical signature of well-organized deep convection. The observed evolution of $Q_1 - Q_2 - Q_{rad}$ shows a distinct eastward tilting structure, illustrating the successive buildup of MSE through vertical subgrid-scale transport: first near the surface via PBL turbulent eddy, then in the lower to mid-troposphere through shallow cumulus, and finally in the upper troposphere via deep convection. While all simulations reproduce the initial phase of this MSE transport reasonably well, their performance diverges in the later stages. CAM_ZMUW and CAM_UNICON lack coherent vertical organization in subgrid-scale MSE transport, despite showing reasonable agreement in Q_1 for CAM_ZMUW and Q_2 for CAM_UNICON. The

21698996, 2026, 4, Downloaded from https://agupubs.onlinelibrary.wiley.com/doi/10.1029/2025JD045016 by Xiaocong Wang , Wiley Online Library on [12/02/2026]. See the Terms and Conditions (https://onlinelibrary.wiley.com/terms-and-conditions) on Wiley Online Library for rules of use; OA articles are governed by the applicable Creative Commons License

21698996, 2026, 4, Downloaded from https://agupubs.onlinelibrary.wiley.com/doi/10.1029/2025JD045016 by Xiaocong Wang , Wiley Online Library on [12/02/2026]. See the Terms and Conditions (https://onlinelibrary.wiley.com/terms-and-conditions) on Wiley Online Library for rules of use; OA articles are governed by the applicable Creative Commons License

enhanced MSE convergence above 500 hPa in CAM_ZMUW suggests that convective-scale transport in the *Zhang-McFarlane* scheme is excessively vigorous. Both CAM_CLUBB and CAM_SP produce well organized tilting structure similar to observations. However, CAM_CLUBB significantly underestimates the magnitude, indicating weak vertical subgrid-scale MSE transport. CAM_SP captures the structure and amplitude more accurately, though it exhibits a premature upper-level MSE convergence maximum—approximately a 6-hr phase lead compared to observations.

4.3. Baroclinic Structure of Heating Coupled With MRG Wave

To better understand how heating at different levels couples with MRG wave structure, we decompose diabatic heating into the first (deep) and second (shallow) baroclinic modes, which are derived using a vertical normal-mode transformation. Mathematically, for a given static stability profile, the solution of the primitive equations linearized about a resting basic state can be decomposed into a superposition of vertical modes. Each mode is algebraically equivalent to a solution of the linearized shallow water equations with a corresponding equivalent depth (Fulton & Schubert, 1985; Žagar et al., 2015). The first and second vertical modes, derived using the mean KWAJEX temperature profile with an upper boundary at 150 hPa, are shown in Figure S2 in Supporting Information S1. By projecting the observed and simulated diabatic heating Q_1 profiles onto the temperature vertical modes, we obtain their corresponding modal decompositions. Figure 8 displays the sum of the first two modes (left column) and their individual contributions (right column). While all simulations reasonably capture the first baroclinic mode, they systematically underestimate the phase lag between the first and second modes during Phases 3 and 4 compared to observations. This discrepancy directly impacts the simulated tilting structure of the MRG wave. For instance, CAM_SP captures the first mode but misses the second, whereas CAM_CLUBB captures the second mode but not the first. CAM_ZMUW reproduces both modes but with a slight delay relative to observations, and CAM_UNICON largely misses the second mode. These differences in the baroclinic heating structure are fundamental to explaining the performance of convectively coupled MRG wave characteristics shown in Figure 7.

5. Sensitivity Experiments

5.1. Sensitivity to CLUBB Configurations

In this subsection, we extend the CAM_CLUBB configuration to two additional setups and investigate their influence on MRG convective coupling. One configuration combines CLUBB with the *Zhang-McFarlane* convection scheme (CAM_CLUBB_ZM), while the other incorporates the stochastic Subgrid Importance Latin Hypercube Sampler (SILHS; Larson & Schanen, 2013; Larson, 2017) to better represent subgrid variability in ice clouds (CAM_CLUBB_SILHS). In practice, SILHS draws four samples from the subgrid PDF at each grid level. Each subcolumn is then passed to the *Morrison-Gettelman* cloud microphysics scheme to compute time tendencies for cloud ice, cloud liquid water, water vapor, and other relevant microphysical variables. Both configurations have been employed in previous studies (Golaz et al., 2019; Qian et al., 2018; Storer et al., 2015; Thayer-Calder et al., 2015; Yang et al., 2020). While the impact on surface precipitation is minor (not shown), the associated diabatic heating shows substantial differences, as illustrated in Figure S3 in Supporting Information S1. Compared to CAM_CLUBB, CAM_CLUBB_ZM produces stronger Q_1, primarily due to excessive deep convective heating. This is accompanied by an overestimation of drying in the lower troposphere. The overall behavior closely resembles that of CAM_ZMUW, highlighting the model's strong sensitivity to deep convection scheme. In contrast, CAM_CLUBB_SILHS produces even weaker Q_1 and Q_2 compared to CAM_CLUBB, particularly in the lower to middle troposphere. The smaller Q_1 and Q_2 are largely attributed to enhanced evaporative cooling process below 500 hPa resulting from the use of SILHS.

The 5-day composites of temperature, moisture and relative humidity for the two additional CLUBB simulations are shown in Figure S4 in Supporting Information S1. Notably, CAM_CLUBB_ZM captures the surface moistening anomaly during Phase 2 reasonably well. However, it also exhibits an unrealistic westward tilt of specific humidity between 400 and 600 hPa, similar to that observed in CAM_ZMUW. The composite fields in CAM_CLUBB_SILHS are nearly identical to those in CAM_CLUBB, indicating that the inclusion of SILHS has a relatively minor impact on MRG simulation. This suggests that although SILHS yields more refined and localized heating profiles, these process-level improvements do not substantially alter the large-scale structure of the MRG wave. The composite anomalies of the apparent heat source Q_1, moisture sink Q_2, and the vertical

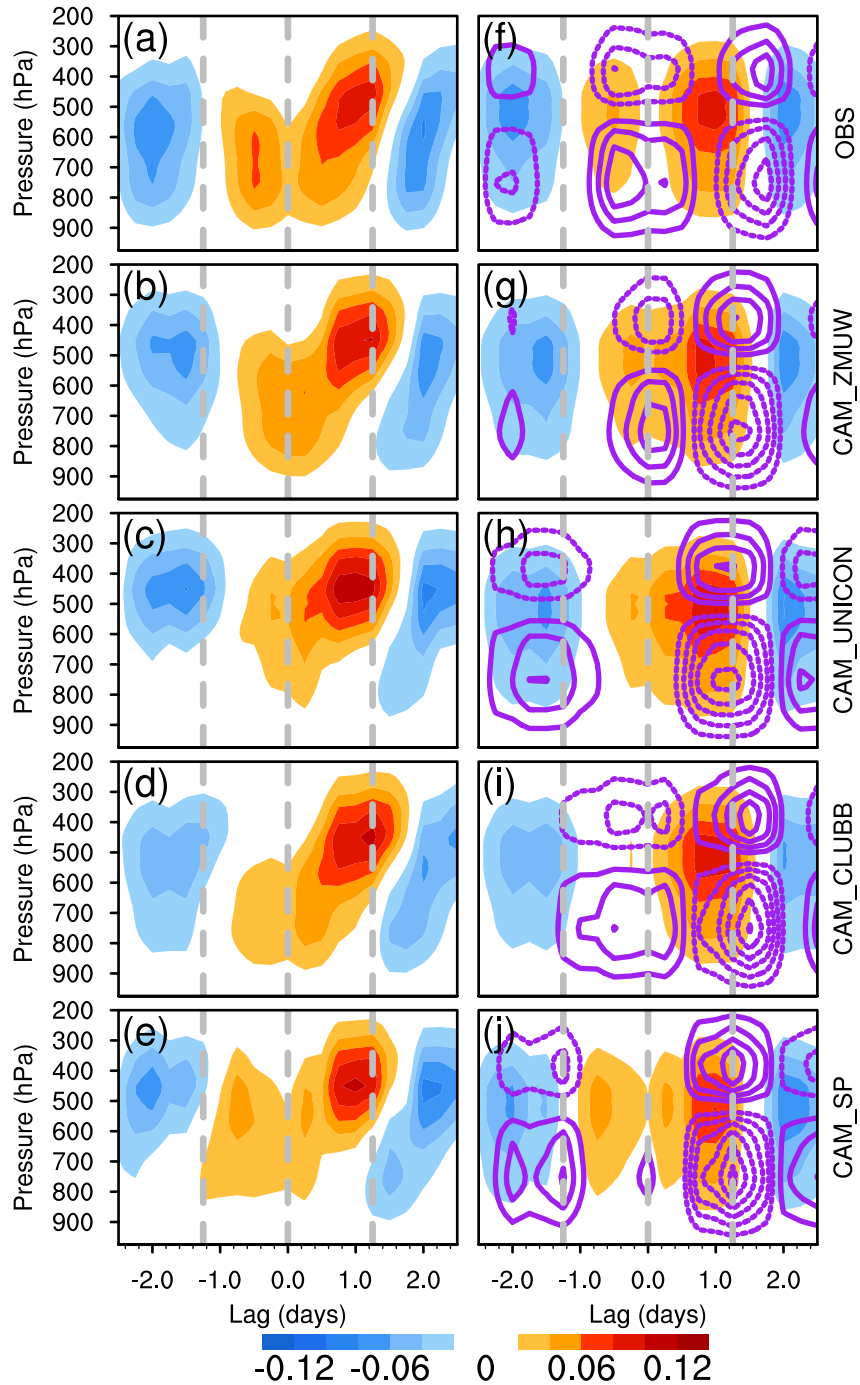


Figure 8. Sum of the first two vertical modes of diabatic heating (Q_1, left column) and their individual modal contributions (right column). In the right column, shading represents the first mode and contours denote the second mode. Units: K/day.

subgrid-scale transport of MSE $Q_1 - Q_2 - Q_{\text{rad}}$ are shown in Figure S5 in Supporting Information S1. Again, the behavior of CAM_CLUBB_ZM closely resembles that of CAM_ZMUW; however, the overestimation of Q_2 is notably reduced in the former. Additionally, the heating structure in CAM_CLUBB_ZM appears more organized, highlighting the advantages of CLUBB over the use of separate PBL turbulence and shallow convection schemes. However, similar to CAM_ZMUW, CAM_CLUBB_ZM still lacks coherent vertical organization in subgrid-scale MSE transport, particularly during the transition from shallow to deep convection. CAM_CLUBB_SILHS produces enhanced Q_1 and Q_2 during Phase 3 compared to CAM_CLUBB, likely due to

21698996, 2026, 4, Downloaded from https://agupubs.onlinelibrary.wiley.com/doi/10.1029/2025JD045016 by Xiaocong Wang , Wiley Online Library on [12/02/2026]. See the Terms and Conditions (https://onlinelibrary.wiley.com/terms-and-conditions) on Wiley Online Library for rules of use; OA articles are governed by the applicable Creative Commons License

21698996, 2026, 4, Downloaded from https://agupubs.onlinelibrary.wiley.com/doi/10.1029/2025JD045016 by Xiaocong Wang, Wiley Online Library on [12/02/2026]. See the Terms and Conditions (https://onlinelibrary.wiley.com/terms-and-conditions) on Wiley Online Library for rules of use; OA articles are governed by the applicable Creative Commons License

the improved representation of ice-phase microphysics enabled by the inclusion of SILHS. Nevertheless, the weak vertical subgrid-scale MSE transport observed in CAM_CLUBB persists in CAM_CLUBB_SILHS.

5.2. Sensitivity to Convective Triggering and Closure Formulations

To examine how convective triggering and closure metrics affect the vertical extent and intensity of parameterized convection, and thereby modulate convective coupling within the MRG wave, two sensitivity experiments were designed. In the first modification, we use the Xie and Zhang (2000) triggering scheme, in which minimum thresholds of positive CAPE and DCAPE are required (70 J/kg and 100 J/kg/h, respectively) to initiate convection. Here, DCAPE is defined as the rate of change of CAPE by large-scale advective tendencies of temperature and water vapor. For the second modification, we replace the standard diluted CAPE closure with an undiluted CAPE closure. The period-averaged diabatic heating and its breakdown by individual parameterization schemes are shown in Figure S6 in Supporting Information S1. Compared to the default configuration, deep convection is more suppressed in the DCAPE triggering experiment, whereas more vigorous in the undiluted CAPE experiment. We notice that shallow convection originating in the boundary layer extends considerably deeper when the DCAPE trigger is applied. This occurs because when deep convection is more suppressed, the plume in the boundary layer can start with larger MSE and become more buoyant when it reaches the middle troposphere. In contrast, the undiluted CAPE closure consumes a larger fraction of the available convective instability, leaving less room for the development of shallow convection. This leads to lower-tropospheric dry bias reduced when the DCAPE trigger is applied, whereas exaggerated with the undiluted CAPE closure (Figure S7 in Supporting Information S1). The composite anomalies of the apparent heat source Q_1, moisture sink Q_2, and the vertical subgrid-scale transport of MSE $Q_1 - Q_2 - Q_{\mathrm{rad}}$ is shown in Figure S8 in Supporting Information S1. As noticed, employing DCAPE as a convective trigger leads to a less organized structure in diabatic heating, with only a marginal congestus heating signal apparent in Phase 2. In contrast, the undiluted CAPE closure produces a more coherent heating structure and exhibits vertically organized subgrid-scale MSE transport. These findings indicate that a more accurate simulation of the background thermodynamic state does not guarantee an improved simulation of convectively coupled MRG waves.

6. Summary

This study evaluates how different physical parameterization schemes in SCAM influence the structure and evolution of convectively coupled MRG waves, using large-scale forcing derived from the TRMM-KWAJEX field campaign. We compare four SCAM configurations: CAM_ZMUW (traditional separate schemes), CAM_UNICON (unified convection scheme), CAM_CLUBB (unified cloud-turbulence framework), and CAM_SP (super-parameterized CAM with embedded cloud-resolving models). Results show that precipitation is broadly similar across all four configurations, but diabatic heating structures exhibit strong sensitivity to parameterization. CAM_ZMUW and CAM_UNICON tend to overestimate both apparent heating Q_1 and moisture sink Q_2, due to excessive deep convection. CAM_CLUBB exhibits weaker vertical transport and underestimates both Q_1 and Q_2, though it compensates with stronger stratiform heating. CAM_SP best matches observations, with errors mostly within ±0.2 K/day. These heating discrepancies then manifest in temperature and moisture biases. CAM_ZMUW and CAM_UNICON exhibit a warm-dry mid-troposphere due to excessive subgrid-scale convective transport, whereas CAM_CLUBB shows a cold-moist bias instead.

When examining the MRG wave structure, all SCMs generally reproduce the observed eastward tilt in temperature and moisture, but notable differences exist. CAM_ZMUW produces an unrealistic westward tilt in moisture between 400 and 600 hPa, while CAM_CLUBB fails to capture the surface moistening anomaly during Phase 2. Only CAM_UNICON and CAM_SP successfully replicate the gradual rise of moisture, closely aligning with the observations. With regard to diabatic heating composites, all SCMs reasonably capture deep convective heating during Phase 3 but struggle to accurately represent cumulus congestus during Phase 2. Only CAM_CLUBB and CAM_SP successfully reproduce the successive vertical subgrid-scale transport of MSE convergence, illustrating a more realistic transition from shallow to deep convection. In contrast, the two configurations employing the mass-flux convection schemes fail to capture this smooth transition. On the other hand, despite its structural realism, CAM_CLUBB underestimates the heating magnitude, reflecting persistently weak vertical subgrid-scale transport of MSE convergence. Further sensitivity experiments reveal that combining CLUBB with the *Zhang-McFarlane* convection scheme results in behavior that closely resembles that of CAM_ZMUW, highlighting the model's strong sensitivity to deep convection scheme. The inclusion of SILHS

leads to enhanced Q_1 and Q_2 during Phase 3 compared to CAM_CLUBB. However, the weak vertical subgrid-scale transport of MSE convergence observed in CAM_CLUBB still remains. To investigate how convective triggering and closure formulations modulate the intensity of parameterized convection and its coupling with the MRG wave, we conducted two sensitivity experiments. Results show applying stricter convective triggering alleviates the lower-tropospheric dry bias, whereas a more liberal closure formulation amplifies it. Nonetheless, a more realistic simulation of the background thermodynamic state does not ensure an improved simulation of the convectively coupled MRG wave.

In summary, this study highlights the strength of super-parameterization in accurately capturing key features of convectively coupled MRG waves, while also revealing varying limitations in both traditional and unified parameterization schemes. The results underscore the need to improve the representation of shallow-to-deep convective transitions in mass-flux schemes and to enhance the vertical subgrid-scale transport within the CLUBB framework.

Conflict of Interest

The authors declare no conflicts of interest relevant to this study.

Data Availability Statement

The KWAJEX large-scale forcing data for driving CAM SCMs, along with all corresponding KWAJEX simulation outputs have been deposited in Zenodo at https://doi.org/10.5281/zenodo.16674464 (Wang et al., 2025).

Acknowledgments
We thank the three anonymous reviewers for their constructive comments that helped to clarify and improve the original paper. This research is jointly supported by the National Key Research and Development Program of China (Grants 2022YFF0802003), the National Natural Science Foundation of China (Grants 42575163, 42175165), the Fundamental Research Funds for the Central Universities NO. 2024300361, and the National Key Scientific and Technological Infrastructure project "Earth System Science Numerical Simulator Facility" (EarthLab).

References

Blossey, P. N., Bretherton, C. S., Cetrone, J., & Kharoutdinov, M. (2007). Cloud-resolving model simulations of KWAJEX: Model sensitivities and comparisons with satellite and radar observations. *Journal of the Atmospheric Sciences*, *64*(5), 1488–1508. https://doi.org/10.1175/JAS3982.1

Bogenschutz, P. A., Gettelman, A., Hannay, C., Larson, V. E., Neale, R. B., Craig, C., & Chen, C.-C. (2018). The path to CAM6: Coupled simulations with CAM5.4 and CAM5.5. *Geoscientific Model Development*, *11*(1), 235–255. https://doi.org/10.5194/gmd-11-235-2018

Bretherton, C. S., & Park, S. (2008). A new bulk shallow-cumulus model and implications for penetrative entrainment feedback on updraft buoyancy. *Journal of the Atmospheric Sciences*, *65*(7), 2174–2193. https://doi.org/10.1175/2007JAS2242.1

Bretherton, C. S., & Park, S. (2009). A new moist turbulence parameterization in the community atmosphere model. *Journal of Climate*, *22*(12), 3422–3448. https://doi.org/10.1175/2008JCLI2556.1

Cheng, Y.-M., Dias, J., Kiladis, G., Feng, Z., & Leung, L. R. (2023). Mesoscale convective systems modulated by convectively coupled equatorial waves. *Geophysical Research Letters*, *50*(10), e2023GL103335. https://doi.org/10.1029/2023GL103335

Clough, S. A., Shephard, M. W., Mlawer, E. J., Delamere, J. S., Iacono, M. J., Cady-Pereira, K., et al. (2005). Atmospheric radiative transfer modeling: A summary of the AER codes. *Journal of Quantitative Spectroscopy and Radiative Transfer*, *91*(2), 233–244. https://doi.org/10.1016/j.jqsrt.2004.05.058

Dias, J., Gehne, M., Kiladis, G. N., & Magnusson, L. (2023). The role of convectively coupled equatorial waves in sub-seasonal predictions. *Geophysical Research Letters*, *50*(21), e2023GL106198. https://doi.org/10.1029/2023GL106198

Dias, J., & Kiladis, G. N. (2019). The influence of tropical forecast errors on higher latitude predictions. *Geophysical Research Letters*, *46*(8), 4450–4459. https://doi.org/10.1029/2019GL082812

Donahue, A. S., & Caldwell, P. M. (2018). Impact of physics parameterization ordering in a global atmosphere model. *Journal of Advances in Modeling Earth Systems*, *10*(2), 481–499. https://doi.org/10.1002/2017MS001067

Feng, T., Yu, J.-Y., Yang, X.-Q., & Huang, R. (2020). Convective coupling in tropical-depression-type waves. Part II: Moisture and moist static energy budgets. *Journal of the Atmospheric Sciences*, *77*, 3423–3440. https://doi.org/10.1175/JAS-D-19-0173.1

Fulton, S. R., & Schubert, W. H. (1985). Vertical normal mode transforms: Theory and application. *Monthly Weather Review*, *113*(4), 647–658. https://doi.org/10.1175/1520-0493(1985)113<0647:vnmtta>2.0.co;2

Gettelman, A., Truesdale, J. E., Bacmeister, J. T., Caldwell, P. M., Neale, R. B., Bogenschutz, P. A., & Simpson, I. R. (2019). The single column atmosphere model version 6 (SCAM6): Not a scam but a tool for model evaluation and development. *Journal of Advances in Modeling Earth Systems*, *11*(5), 1381–1401. https://doi.org/10.1029/2018MS001578

Golaz, J., Caldwell, P. M., Van Roekel, L. P., Petersen, M. R., Tang, Q., Wolfe, J. D., et al. (2019). The DOE E3SM coupled model version 1: Overview and evaluation at standard resolution. *Journal of Advances in Modeling Earth Systems*, *11*(7), 2089–2129. https://doi.org/10.1029/2018MS001603

Golaz, J.-C., Larson, V. E., & Cotton, W. R. (2002). A PDF-based model for boundary layer clouds. Part I: Method and model description. *Journal of the Atmospheric Sciences*, *59*(24), 3540–3551. https://doi.org/10.1175/1520-0469(2002)059<3540:APBMFB>2.0.CO;2

Guo, H., Golaz, J.-C., Donner, L. J., Wyman, B., Zhao, M., & Ginoux, P. (2015). CLUBB as a unified cloud parameterization: Opportunities and challenges. *Geophysical Research Letters*, *42*(11), 4540–4547. https://doi.org/10.1002/2015GL063672

Guo, Z., Griffin, B. M., Domke, S., & Larson, V. E. (2021). A parameterization of turbulent dissipation and pressure damping time scales in stably stratified inversions, and its effects on low clouds in global simulations. *Journal of Advances in Modeling Earth Systems*, *13*(4), e2020MS002278. https://doi.org/10.1029/2020MS002278

Huang, P., Chou, C., & Huang, R. (2013). The activity of convectively coupled equatorial waves in CMIP3 global climate models. *Theoretical and Applied Climatology*, *112*(3), 697–711. https://doi.org/10.1007/s00704-012-0761-4

Hung, M.-P., Lin, J.-L., Wang, W., Kim, D., Shinoda, T., & Weaver, S. J. (2013). MJO and convectively coupled equatorial waves simulated by CMIP5 climate models. *Journal of Climate*, *26*(17), 6185–6214. https://doi.org/10.1175/JCLI-D-12-00541.1

21698996, 2026, 4, Downloaded from https://agupubs.onlinelibrary.wiley.com/doi/10.1029/2025JD045016 by Xiaocong Wang , Wiley Online Library on [12/02/2026]. See the Terms and Conditions (https://onlinelibrary.wiley.com/terms-and-conditions) on Wiley Online Library for rules of use; OA articles are governed by the applicable Creative Commons License

Khairoutdinov, M. F., & Randall, D. A. (2001). A cloud resolving model as a cloud parameterization in the NCAR Community Climate System Model: Preliminary results. *Geophysical Research Letters*, *28*(18), 3617–3620. https://doi.org/10.1029/2001GL013552

Khairoutdinov, M. F., & Randall, D. A. (2003). Cloud resolving modeling of the ARM summer 1997 IOP: Model formulation, results, uncertainties, and sensitivities. *Journal of the Atmospheric Sciences*, *60*(4), 607–625. https://doi.org/10.1175/1520-0469(2003)060<0607:CRMOTA>2.0.CO;2

Kiladis, G. N., Wheeler, M. C., Haertel, P. T., Straub, K. H., & Roundy, P. E. (2009). Convectively coupled equatorial waves. *Reviews of Geophysics*, *47*(2). https://doi.org/10.1029/2008RG000266

Krishnamurti, T. N., Gnanaseelan, C., & Chakraborty, A. (2007). Prediction of the diurnal change using a multimodel superensemble. Part I: Precipitation. *Monthly Weather Review*, *135*(10), 3613–3632. https://doi.org/10.1175/MWR3446.1

Kuang, Z. (2008). A moisture-stratiform instability for convectively coupled waves. *Journal of the Atmospheric Sciences*, *65*(3), 834–854. https://doi.org/10.1175/2007JAS2444.1

Larson, V. E. (2017). CLUBB-SILHS: A parameterization of subgrid variability in the atmosphere. *arXiv preprint arXiv:1711.03675*. https://doi.org/10.48550/arXiv.1711.03675

Larson, V. E., Golaz, J.-C., & Cotton, W. R. (2002). Small-scale and mesoscale variability in cloudy boundary layers: Joint probability density functions. *Journal of the Atmospheric Sciences*, *59*(24), 3519–3539. https://doi.org/10.1175/1520-0469(2002)059<3519:SSAMVI>2.0.CO;2

Larson, V. E., & Schanen, D. P. (2013). The subgrid importance latin hypercube sampler (SILHS): A multivariate subcolumn generator. *Geoscientific Model Development*, *6*(5), 1813–1829. https://doi.org/10.5194/gmd-6-1813-2013

Lin, G., Ghan, S. J., Wang, M., Ma, P.-L., Easter, R. C., Ovchinnikov, M., et al. (2018). Development and evaluation of an explicit treatment of aerosol processes at cloud scale within a multi-scale modeling framework (MMF). *Journal of Advances in Modeling Earth Systems*, *10*(7), 1663–1679. https://doi.org/10.1029/2018MS001287

Lin, J.-L., Kiladis, G. N., Mapes, B. E., Weickmann, K. M., Sperber, K. R., Lin, W., et al. (2006). Tropical intraseasonal variability in 14 IPCC AR4 climate models. Part I: Convective signals. *Journal of Climate*, *19*(12), 2665–2690. https://doi.org/10.1175/JCLI3735.1

Lin, L., Gettelman, A., Xu, Y., Wu, C., Wang, Z., Rosenbloom, N., et al. (2019). CAM6 simulation of mean and extreme precipitation over Asia: Sensitivity to upgraded physical parameterizations and higher horizontal resolution. *Geoscientific Model Development*, *12*(8), 3773–3793. https://doi.org/10.5194/gmd-12-3773-2019

Lin, Y.-L., Farley, R. D., & Orville, H. D. (1983). Bulk parameterization of the snow field in a cloud model. *Journal of Applied Meteorology and Climatology*, *22*(6), 1065–1092. https://doi.org/10.1175/1520-0450(1983)022<1065:BPOTSF>2.0.CO;2

Ma, H., Zhang, K., Tang, S., Xie, S., & Fu, R. (2021). Evaluation of the causes of Wet-Season dry biases Over Amazonia in CAM5. *Journal of Geophysical Research: Atmospheres*, *126*(11), e2020JD033859. https://doi.org/10.1029/2020JD033859

Majda, A. J., & Shefter, M. G. (2001). Models for stratiform instability and convectively coupled waves. *Journal of the Atmospheric Sciences*, *58*(12), 1567–1584. https://doi.org/10.1175/1520-0469(2001)058<1567:MFSIAC>2.0.CO;2

Mapes, B. E. (2000). Convective inhibition, subgrid-scale triggering energy, and stratiform instability in a toy tropical wave model. *Journal of the Atmospheric Sciences*, *57*(10), 1515–1535. https://doi.org/10.1175/1520-0469(2000)057<1515:cisste>2.0.co;2

Morrison, H., Curry, J. A., & Khvorostyanov, V. I. (2005). A new double-moment microphysics parameterization for application in cloud and climate models. Part I: Description. *Journal of the Atmospheric Sciences*, *62*(6), 1665–1677. https://doi.org/10.1175/JAS3446.1

Morrison, H., & Gettelman, A. (2008). A new two-moment bulk stratiform cloud microphysics scheme in the community atmosphere model, version 3 (CAM3). Part I: Description and numerical tests. *Journal of Climate*, *21*(15), 3642–3659. https://doi.org/10.1175/2008JCLI2105.1

Neggers, R. A. J., Köhler, M., & Beljaars, A. C. M. (2009). A dual mass flux framework for boundary layer convection. Part I: Transport. *Journal of the Atmospheric Sciences*, *66*(6), 1465–1487. https://doi.org/10.1175/2008JAS2635.1

Park, S. (2014a). A unified convection scheme (UNICON). Part I: Formulation. *Journal of the Atmospheric Sciences*, *71*(11), 3902–3930. https://doi.org/10.1175/JAS-D-13-0233.1

Park, S. (2014b). A unified convection scheme (UNICON). Part II: Simulation. *Journal of the Atmospheric Sciences*, *71*(11), 3931–3973. https://doi.org/10.1175/JAS-D-13-0234.1

Park, S., & Bretherton, C. S. (2009). The University of Washington shallow convection and moist turbulence schemes and their impact on climate simulations with the community atmosphere model. *Journal of Climate*, *22*(12), 3449–3469. https://doi.org/10.1175/2008jcli2557.1

Park, S., Bretherton, C. S., & Rasch, P. J. (2014). Integrating cloud processes in the community atmosphere model, version 5. *Journal of Climate*, *27*(18), 6821–6856. https://doi.org/10.1175/JCLI-D-14-00087.1

Qian, Y., Wan, H., Yang, B., Golaz, J.-C., Harrop, B., Hou, Z., et al. (2018). Parametric sensitivity and uncertainty quantification in the version 1 of E3SM atmosphere model based on short perturbed parameter ensemble simulations. *Journal of Geophysical Research: Atmospheres*, *123*(23), 13046–13073. https://doi.org/10.1029/2018JD028927

Randall, D. A., Xu, K., Somerville, R. J. C., & Iacobellis, S. (1996). Single-column models and cloud ensemble models as links between observations and climate models. *Journal of Climate*, *9*(8), 1683–1697. https://doi.org/10.1175/1520-0442(1996)009<1683:SCMACE>2.0.CO;2

Schreck, C. J., Janiga, M. A., & Baxter, S. (2020). Sources of tropical subseasonal skill in the CFSv2. *Monthly Weather Review*, *148*(4), 1553–1565. https://doi.org/10.1175/MWR-D-19-0289.1

Schumacher, C., Ciesielski, P. E., & Zhang, M. H. (2008). Tropical cloud heating profiles: Analysis from KWAJEX. *Monthly Weather Review*, *136*(11), 4289–4300. https://doi.org/10.1175/2008MWR2275.1

Schumacher, C., Zhang, M. H., & Ciesielski, P. E. (2007). Heating structures of the TRMM field campaigns. *Journal of the Atmospheric Sciences*, *64*(7), 2593–2610. https://doi.org/10.1175/JAS3938.1

Sobel, A. H., & Bretherton, C. S. (2000). Modeling tropical precipitation in a single column. *Journal of Climate*, *13*(24), 4378–4392. https://doi.org/10.1175/1520-0442(2000)013<4378:MTPIAS>2.0.CO;2

Sobel, A. H., Yuter, S. E., Bretherton, C. S., & Kiladis, G. N. (2004). Large-scale meteorology and deep convection during TRMM KWAJEX. *Monthly Weather Review*, *132*(2), 422–444. https://doi.org/10.1175/1520-0493(2004)132<0422:LMADCD>2.0.CO;2

Storer, R. L., Griffin, B. M., Höft, J., Weber, J. K., Raut, E., Larson, V. E., et al. (2015). Parameterizing deep convection using the assumed probability density function method. *Geoscientific Model Development*, *8*(1), 1–19. https://doi.org/10.5194/gmd-8-1-2015

Straub, K. H., & Kiladis, G. N. (2003). The observed structure of convectively coupled kelvin waves: Comparison with simple models of coupled wave instability. *Journal of the Atmospheric Sciences*, *60*(14), 1655–1668. https://doi.org/10.1175/1520-0469(2003)060<1655:TOSOCC>2.0.CO;2

Swann, A., Sobel, A. H., Yuter, S. E., & Kiladis, G. N. (2006). Observed radar reflectivity in convectively coupled kelvin and mixed rossby-gravity waves. *Geophysical Research Letters*, *33*(10). https://doi.org/10.1029/2006GL025979

Tang, S., & Zhang, M. (2015). Three-dimensional constrained variational analysis: Approach and application to analysis of atmospheric diabatic heating and derivative fields during an ARM SGP intensive observational period. *Journal of Geophysical Research: Atmospheres*, *120*(15), 7283–7299. https://doi.org/10.1002/2015JD023621

21698996, 2026, 4, Downloaded from https://agupubs.onlinelibrary.wiley.com/doi/10.1029/2025JD045016 by Xiaocong Wang , Wiley Online Library on [12/02/2026]. See the Terms and Conditions (https://onlinelibrary.wiley.com/terms-and-conditions) on Wiley Online Library for rules of use; OA articles are governed by the applicable Creative Commons License

Tang, S., Zhang, M., & Xie, S. (2017). Investigating the dependence of SCM simulated precipitation and clouds on the spatial scale of large-scale forcing at SGP. *Journal of Geophysical Research: Atmospheres*, *122*(16), 8724–8738. https://doi.org/10.1002/2017JD026565

Thayer-Calder, K., Gettelman, A., Craig, C., Goldhaber, S., Bogenschutz, P. A., Chen, C.-C., et al. (2015). A unified parameterization of clouds and turbulence using CLUBB and subcolumns in the community atmosphere model. *Geoscientific Model Development*, *8*(12), 3801–3821. https://doi.org/10.5194/gmd-8-3801-2015

Wang, L., & Li, T. (2017). Convectively coupled kelvin waves in CMIP5 coupled climate models. *Climate Dynamics*, *48*(3), 767–781. https://doi.org/10.1007/s00382-016-3109-4

Wang, M., Ghan, S., Easter, R., Ovchinnikov, M., Liu, X., Kassianov, E., et al. (2011). The multi-scale aerosol-climate model PNNL-MMF: Model description and evaluation. *Geoscientific Model Development*, *4*(1), 137–168. https://doi.org/10.5194/gmd-4-137-2011

Wang, X. (2015). Development of a toy column model and its application in testing cumulus convection parameterizations. *Science Bulletin*, *60*(15), 1359–1365. https://doi.org/10.1007/s11434-015-0850-8

Wang, X. (2022). Role of cloud subgrid-scale structure in modulating clouds viewed by ISCCP, MODIS, and MISR simulators. *Journal of Geophysical Research: Atmospheres*, *127*(11), e2021JD036378. https://doi.org/10.1029/2021JD036378

Wang, X., Liu, Y., Zhang, M., Liu, Y., Tang, S., Guo, Z., et al. (2025). CAM SCM simulations for the KWAJEX field campaign [Dataset]. *Zenodo*. https://doi.org/10.5281/zenodo.16674464

Wang, X., & Zhang, M. (2013). An analysis of parameterization interactions and sensitivity of single-column model simulations to convection schemes in CAM4 and CAM5. *Journal of Geophysical Research: Atmospheres*, *118*(16), 8869–8880. https://doi.org/10.1002/jgrd.50690

Wang, X., & Zhang, M. (2015). The coupling of mixed rossby-gravity waves with diabatic heating during the TRMM-KWAJEX field campaign. *Geophysical Research Letters*, *42*(19), 8241–8249. https://doi.org/10.1002/2015GL065813

Wang, X., & Zhang, M. (2024). Convectively coupled Rossby-Gravity waves in a field campaign: How they are captured in reanalysis products. *Atmospheric Science Letters*, *25*(4), e1206. https://doi.org/10.1002/asl.1206

Wang, Y.-C., Pan, H.-L., & Hsu, H.-H. (2015). Impacts of the triggering function of cumulus parameterization on warm-season diurnal rainfall cycles at the atmospheric radiation measurement southern Great Plains site. *Journal of Geophysical Research: Atmospheres*, *120*(20), 10681–10702. https://doi.org/10.1002/2015JD023337

Xie, S., Ma, H.-Y., Boyle, J. S., Klein, S. A., & Zhang, Y. (2012). On the correspondence between short- and long-time-scale systematic errors in CAM4/CAM5 for the year of tropical convection. *Journal of Climate*, *25*(22), 7937–7955. https://doi.org/10.1175/JCLI-D-12-00134.1

Xie, S., & Zhang, M. (2000). Impact of the convection triggering function on single-column model simulations. *Journal of Geophysical Research*, *105*(D11), 14983–14996. https://doi.org/10.1029/2000JD900170

Yang, B., Wang, M., Zhang, G. J., Guo, Z., Qian, Y., Huang, A., & Zhang, Y. (2020). Simulated precipitation diurnal variation with a deep convective closure subject to shallow convection in community atmosphere model Version 5 coupled with CLUBB. *Journal of Advances in Modeling Earth Systems*, *12*(7), e2020MS002050. https://doi.org/10.1029/2020MS002050

Yuan, W., Yu, R., Zhang, M., Lin, W., Li, J., & Fu, Y. (2013). Diurnal cycle of summer precipitation over subtropical east Asia in CAM5. *Journal of Climate*, *26*(10), 3159–3172. https://doi.org/10.1175/JCLI-D-12-00119.1

Žagar, N., Kasahara, A., Terasaki, K., Tribbia, J., & Tanaka, H. (2015). Normal-mode function representation of global 3-D data sets: Open-access software for the atmospheric research community. *Geoscientific Model Development*, *8*(4), 1169–1195. https://doi.org/10.5194/gmd-8-1169-2015

Zhang, G. J., & McFarlane, N. A. (1995). Sensitivity of climate simulations to the parameterization of cumulus convection in the canadian climate centre general circulation model. *Atmosphere-Ocean*, *33*(3), 407–446. https://doi.org/10.1080/07055900.1995.9649539

Zhang, M. H., & Lin, J. L. (1997). Constrained variational analysis of sounding data based on column-integrated budgets of mass, heat, moisture, and momentum: Approach and application to ARM measurements. *Journal of the Atmospheric Sciences*, *54*(11), 1503–1524. https://doi.org/10.1175/1520-0469(1997)054<1503:CVAOSD>2.0.CO;2

Zhang, M. H., Lin, J. L., Cederwall, R. T., Yio, J. J., & Xie, S. C. (2001). Objective analysis of ARM IOP data: Method and sensitivity. *Monthly Weather Review*, *129*(2), 295–311. https://doi.org/10.1175/1520-0493(2001)129<0295:OAOAID>2.0.CO;2

Zhao, Y., Wang, X., Liu, Y., & Wu, G. (2024). Are parameterized entrainment rates as scale dependent as those estimated from cloud resolving model simulations? *Geophysical Research Letters*, *51*(19), e2024GL110735. https://doi.org/10.1029/2024GL110735

21698996, 2026, 4, Downloaded from https://agupubs.onlinelibrary.wiley.com/doi/10.1029/2025JD045016 by Xiaocong Wang , Wiley Online Library on [12/02/2026]. See the Terms and Conditions (https://onlinelibrary.wiley.com/terms-and-conditions) on Wiley Online Library for rules of use; OA articles are governed by the applicable Creative Commons License